A Developmentally Regulated Two-Step Process Generates a Noncentrosomal Microtubule Network in Drosophila Tracheal Cells

Véronique Brodu, Alexandre D Baffet, Pierre-Marie Le Droguen, Jordi Casanova, Antoine Guichet

Developmental Cell
Article

A Developmentally Regulated Two-Step Process Generates a Noncentrosomal Microtubule Network in *Drosophila* Tracheal Cells

Véronique Brodu,[1,*] Alexandre D. Baffet,[1] Pierre-Marie Le Droguen,[1] Jordi Casanova,[2,3,4,*] and Antoine Guichet[1,4]
[1]Institut Jacques Monod- CNRS, 15 Rue H. Brion, 75205 Paris Cedex 13, France
[2]Institut de Biologia Molecular de Barcelona-CSIC
[3]Institut de Recerca Biomèdica de Barcelona
Baldiri Reixac 10-12, 08028 Barcelona, Spain
[4]These authors contributed equally to this work
*Correspondence: brodu.veronique@ijm.univ-paris-diderot.fr (V.B.), jordi.casanova@ibmb.csic.org (J.C.)
DOI 10.1016/j.devcel.2010.03.015

SUMMARY

Microtubules (MTs) are essential for many cell features, such as polarity, motility, shape, and vesicle trafficking. Therefore, in a multicellular organism, their organization differs between cell types and during development; however, the control of this process remains elusive. Here, we show that during *Drosophila* tracheal morphogenesis, MT reorganization is coupled to relocalization of the microtubule organizing centers (MTOC) components from the centrosome to the apical cell domain from where MTs then grow. We reveal that this process is controlled by the *trachealess* patterning gene in a two-step mechanism. MTOC components are first released from the centrosome by the activity of the MT-severing protein Spastin, and then anchored apically through the transmembrane protein Piopio. We further show that these changes are essential for tracheal development, thus stressing the functional relevance of MT reorganization for morphogenesis.

INTRODUCTION

MT cytoskeleton plays essential roles in determining cell shape, cell polarity, and vesicle trafficking. As a consequence, MT reorganization during differentiation is essential for morphogenesis. MTs are filamentous polymers composed of α- and β-tubulin heterodimers and form highly organized, polarized networks. MT formation takes place primarily at morphologically distinct structures termed microtubule organizing centers (MTOCs) (Pickett-Heaps, 1971; Wiese and Zheng, 2006). In most animal cells, polarized arrays of MTs are nucleated from the centrosome, an organelle composed of a pair of centrioles that recruits and organizes a large number of proteins to form the pericentriolar material (PCM). Within the PCM, many proteins assemble into a scaffold that docks the γ-tubulin ring complex (γ-TuRC), which nucleates and controls MT growth (Raynaud-Messina and Merdes, 2007). The γ-TuRC is composed of γ-tubulin and highly conserved factors named Grips (from gamma-tubulin ring proteins) (Oegema et al., 1999) that are distinctly organized. First, Dgrip84 and Dgrip91 together with γ-Tubulin assemble into the γ-tubulin small complex (γ-TuSC) (Wiese and Zheng, 2006). Then, outer Dgrip subunits (Dgrip75, Dgrip128, and Dgrip163, for example) associate with the γ-TuSC, thus organizing the γ-TuRC (Wiese and Zheng, 2006), although these outer Dgrip subunits are nor necessary to target γ-tubulin to centrosomes (Verollet et al., 2006). However, in many cell types, MTs are not associated with the centrosome (Keating and Borisy, 1999). Noncentrosomal arrays of MTs are frequently generated in differentiated cells and are likely to expand the functional repertoire of the MT cytoskeleton. This is particularly true during the differentiation of specialized cell types in multicellular organisms (for review see Bartolini and Gundersen, 2006). The relocation of MT-anchoring proteins to noncentrosomal sites, such as the apical cell surface, occurs during the development of numerous tissues. But the mechanisms that regulate this process and its function are poorly understood.

We studied the control of MT nucleation and organization and its role in morphogenetic processes during tracheal formation in *Drosophila*, a well-established model used to study the development of organs with complex tubular structures (Affolter et al., 2003). The tracheal system arises from clusters of ectodermal cells or tracheal placodes at each side of ten embryonic segments. By stage 11, cells of each tracheal placode invaginate to form a sac-like structure that generates a luminal cavity and thereafter migrate to form the different tracheal branches, which, by stage 13, fuse with those of adjacent metameres (Uv et al., 2003). Importantly, once tracheal cells invaginate, there is no further cell division.

In this study, we uncover a regulatory mechanism orchestrating the formation of noncentrosomal arrays of microtubules in an in vivo developmental context. We demonstrate that this mechanism requires γ-TuRC apical relocalization and is controlled in a two-step process by Trachealess (Trh), a transcription factor specifying tracheal fate. First, it proceeds with a Spastin-mediated release from the centrosome and second with a Piopio-mediated anchoring in the apical membrane. Finally, we reveal the functional significance of MT reorganization during organ formation in a living organism.

RESULTS

MT Network Organization in Tracheal Cells and Changes in MT Subnetworks during Development

We first characterized MT organization during tracheal morphogenesis. In invaginating placodes and throughout tracheal development, the nucleus is basally located, the apical domain faces the lumen, and centrosomes localize within a subapical domain (Figures 1A–1F). As reported in other epithelial cell types (Bartolini and Gundersen, 2006), an apical array of short MTs, organized into a meshwork, forms a cap-like structure at the apical domain whereas long MT fibers are distributed along the basolateral cell domain (Figures 1B, 1C, 1E, and 1F). We observed that α-tubulin levels, and therefore relative levels of MT (see Experimental Procedures), are 2-fold higher in tracheal metameres compared with the surrounding epithelial cells and these levels remain constant during tracheal morphogenesis (Figure 1K). We subsequently examined tyrosination, which is associated with newly assembled MT fibers, and α-tubulin posttranslational modifications such as acetylation, which occurs on stable MT fibers (Hammond et al., 2008). At stage 11, most MTs contain tyrosinated tubulin (referred as tyr-MT) (Figures 1G, 1G″, and 1L) and appear as long fibers along the basolateral domain. Conversely, the level of acetylated-tubulin in MTs (ace-MT) is low (Figures 1I, 1I″, and 1L) and ace-MTs are significantly shorter than tyr-MTs (Figures 1G′ and 1I′). From stage 13, tyr-MT levels gradually decrease whereas ace-MT levels progressively increase (Figures 1H–1J″ and 1L). This observation suggests a progressive decrease in MT nucleation activity and an increase in MT stabilization during tracheal morphogenesis.

γ-TuRC Is Apically Relocalized in Tracheal Cells during Invagination

γ-Tubulin colocalizes with centrosomes in the ectoderm before tracheal specification and remains at centriole-containing centrosomes in surrounding epithelial cells (Figure 2A, arrowheads). However, γ-tubulin is no longer associated with centrioles in the invaginating tracheal cells and later on (Figures 2A′ and 2K; see Figures S1A–S1D available online and data not shown). The same is true for Dgrip84, a γ-TuSC component, which besides a cytoplasmic distribution colocalizes with centrosomes in epidermal (Figures 2H and 2H″) and tracheal cells before invagination (Figures 2B–2B‴) but is largely and gradually removed from centrioles during this process (Figures 2C–E‴ and 2K). By the end of invagination, Dgrip84 and γ-tubulin are localized just below Crumbs, a marker of the apical cell domain (Figures 2F and 2G; data not shown). Dgrip84 apical localization persists throughout tracheal morphogenesis (Figures 1E–E‴ and Figures S1K and S1K′). Initial Dgrip84 apical relocalization is MT-dependent, as indicated by its loss either by Spastin (Spas) overexpression, which has efficiently been used to disassemble MTs (Jankovics and Brunner, 2006; Sherwood et al., 2004), or by cold treatment to depolymerize MTs (Figures S1G, S1G′, S1J, and S1J′). Furthermore, Dgrip84 apical distribution is restored when MTs are reassembled (Figures S1H–S1I″). However, from stage 12, the apical localization of Dgrip84 is not compromised when MTs are disassembled (Figures S1K–S1L′), which suggests a multistep mechanism of γ-TuRC repositioning. Similar results were obtained with Dgrip91, the other γ-TuSC component (not shown). In addition, we also observed an apical localization of Dgrip75 (data not shown) and Dgrip163 (Figures S1E–S1F′) in the tracheal cells during branching process, indicating that not only the γ-TuSC but the whole γ-TuRC is apically relocalized in tracheal cells during invagination where it remains during tracheal morphogenesis.

MT Nucleation Center Shifts from Centriole Position to Cell Apical Domain during Tracheal Morphogenesis

We then addressed whether the change in γ-TuRC localization implied a shift in MT nucleation activity. Alternatively, MTs might still be nucleated at the centrosomes and then released together with the γ-TuRC and apically anchored (Keating and Borisy, 1999). We depolymerized MTs by cold treatment and monitored their regrowth over 2 min in tracheal cells (Figures 3B–3M′; Figure S2) compared to epithelial cells (Figures 3N–3S′). To identify the MT nucleation center, we defined areas of maximum intensity for tyrosinated tubulin signal (see Experimental Procedures and Figures 3A, 3C, 3F, 3I, 3L, 3O, and 3R, colored outline) and then compared it with the centriole position (Figures 3D, 3G, 3J, 3M, 3P, and 3S, green dots) and quantified their overlap (Figure 3T). In tracheal cells of stage 11, centrioles lie within the maximum intensity domain in 87% of untreated controls and in 89.5% of 2 min regrowth; in the remaining cases, they partially overlap but are never apart (Figures 3D′, 3G′, and 3T). In contrast, in tracheal cells of stage 13, the maximum intensity areas lie in the apical domain and not at centrioles in 84.2% of untreated controls and 69.2% of 2 min regrowth (Figures 3J′, 3M′, and 3T). Furthermore, areas occupied by the maximum intensity signal are significantly larger at stage 13 than at stage 11 (data not shown). The shift in MT regrowth activity is specific to tracheal cells. In epidermal cells, maximum intensity domains overlap predominantly with centrosomes. Indeed, at stage 11 (data not shown) or stage 13 (Figures 3P′ and 3S′), in almost all the cases centrioles lie within the maximum intensity domain (Figure 3T). Together with the change in γ-TuRC localization, these results strongly suggest that, in tracheal cells, MT nucleation activity is associated with centriole-containing centrosomes at stage 11 and shifts to the apical domain by stage 13 while it remains at centriole-containing centrosomes in overlaying epithelial cells.

Piopio Contributes to the γ-TuRC Apical Anchoring

We next aimed to identify the molecular effectors required for MT reorganization. *trh* codes for a transcription factor that triggers tracheal development (Isaac and Andrew, 1996; Wilk et al., 1996). We therefore examined whether MT changes in tracheal cells were a consequence of tracheal fate specification. Indeed, relocalization of γ-tubulin and Dgrip84 are impaired in *trh* mutant cells (Figures 2I–2J‴ and 2K). Similarly, the higher MT levels observed in wild-type are not detected in *trh* mutants (Figure 1K). Thus, MT reorganization in tracheal cells is associated with their fate specification and is ultimately controlled by the activity of *trh*.

We thus searched for *trh*-regulated mechanisms and considered Piopio (Pio) a good candidate for a γ-TuRC anchoring factor. Pio is a transmembrane protein that contributes to tracheal branch extension, and in wing epithelial cells it is required for MT organization (Bokel et al., 2005). *pio* is expressed

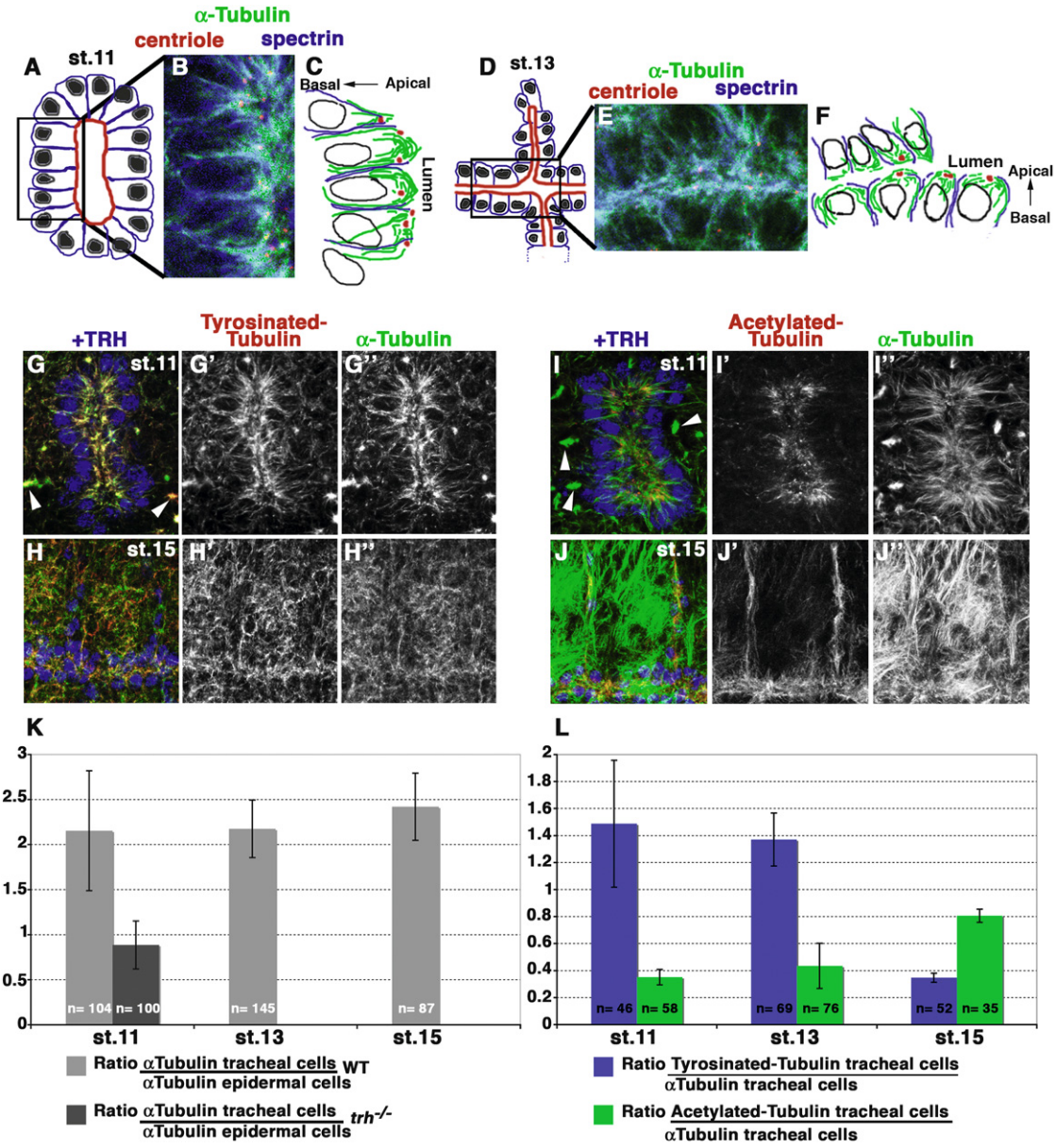

Figure 1. MT Organization and Changes in MT Subnetworks during Tracheal Development

(A–F) MT distribution and centriole position within tracheal cells at stages 11 (A–C) and 13 (D–F). (A and D) Schematic representation of a tracheal placode ([A], stage 11) and of the dorsal part of a tracheal metamere ([D], stage 13). Apical side of tracheal cells, facing the lumen, appears in red and their nuclei are basally located (B, C, E, and F). (C) and (F) are schematic representations of an enlarged view of (B) and (E), respectively. Anti-α-tubulin labels the MT network, centrioles are detected by an anti-GFP antibody on asl-YFP embryos, and anti-spectrin labels cell membranes. Here and in the rest of the figures, anterior is to the left and dorsal is to the top.

(G–J″) Dynamics of posttranslational modifications of α-tubulin and α-tubulin contents using anti-tyrosinated tubulin (G-H″) and anti-acetylated tubulin (I-J″), respectively, at stages 11 (G and I) and 15 (H and J) and their respective quantifications (K and L). Note that epithelial cells are dividing (arrowheads, [G and I]) while tracheal cells have already stopped dividing.

(K) Graph showing ratios between values of signal intensity for α-tubulin at stages 11, 13, and 15 of WT embryos (gray bars) and at stage 11 of *trh* mutant embryos (dark gray bar) (see Experimental Procedures).

(L) Graph showing ratios between values of signal intensity for tyrosinated tubulin (blue bars) and acetylated tubulin (green bars) of WT stage 11, 13, and 15. Error bars indicate standard deviation.

in the tracheal placodes under *trh* control (Figure 4A). In addition, ectopic Trh expression driven by *arm*GAL4 leads to ectopic expression of Pio in dorsal epidermal cells (Figure 4B). Furthermore, ectopic Trh expression under a *sal*GAL4 driver is able to induce Pio expression at specific positions where Trh has the capacity to induce its target genes (Boube et al., 2000) (Figure 4C). Altogether, these results indicate that Trh regulates *pio* expression. Although these results do not indicate whether

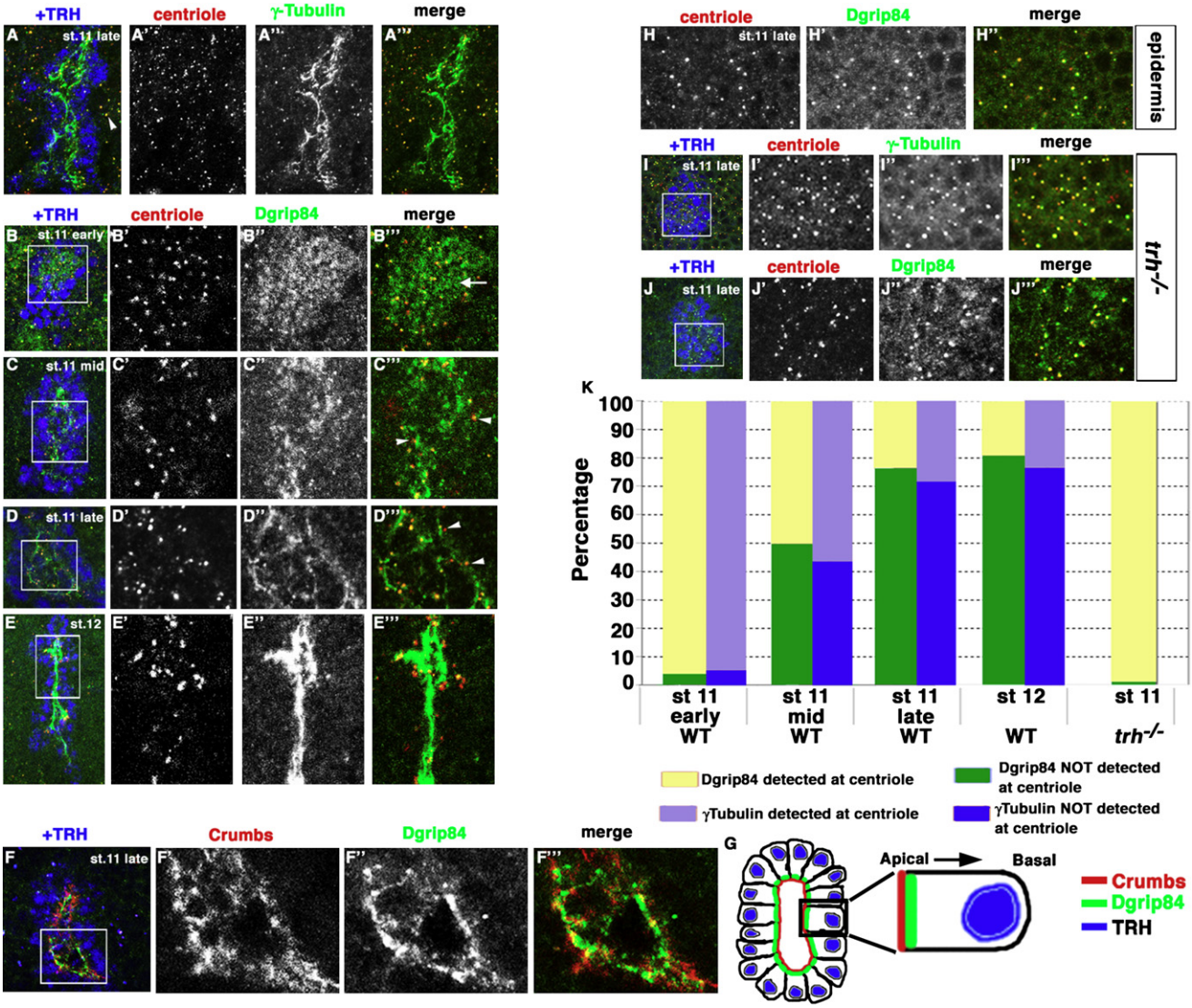

Figure 2. The Apical Translocation of MT Nucleation Activity during Invagination Is *trh* Dependent

(A) At late stage 11, γ-tubulin colocalizes with the centriole position in epithelial cells surrounding tracheal cells (arrowhead). In contrast, in tracheal cells, γ-tubulin is mostly distributed outside centriole location (A′–A″′).

(B–E″′) Dynamics of Dgrip84 relocalization in tracheal placode invagination during stages 11 and 12. At early stage 11, Dgrip84 colocalizes with centrioles in tracheal and epithelial cells (B–B″′). In addition, a more diffuse Dgrip84 staining is restricted to a small group of tracheal cells that have initiated invagination ([B″′], arrows). At mid-stage 11 (C–C″′), some centrioles are depleted in Dgrip84 (arrowheads) and others present a lower Dgrip84 detection level. A large part of the Dgrip84 signal is distributed in cytoplasm. At the end of invagination (D–D″′), most centrioles are depleted in Dgrip84 (arrowheads). (E–E″′) At stage 12, Dgrip84 is mostly detected apically in the tracheal cells. Only a few centrioles contain Dgrip84.

(F–F″′) At late stage 11, Dgrip84 colocalizes with the Crumbs-containing apical domain.

(G) Schematic representation of Crumbs and Dgrip84 apical distribution in tracheal cells at placode stage.

(H–H″) In epidermal cells, Dgrip84 colocalizes perfectly with centrioles.

(I–J″′) Remarkably, γ-tubulin (I–I″′) and Dgrip84 (J–J″′) colocalization with the centriole are restored in *trh* mutant tracheal cells and are then identical to epidermal cells (H-H″′).

(K) Plot showing percentage of centriole colocalizing (in yellow) or not (in green) with Dgrip84 from early stage 11 to stage 12 of WT embryos and of stage 11 *trh* mutant embryos. Plot also showing percentage of centriole colocalizing (in purple) or not (in blue) with γ-tubulin from early stage 11 to stage 12 of WT embryos. See also Figure S1.

pio is a direct *trh* target gene, we note that there are *trh* binding sites in the *D. melanogaster pio* promoter that are also present in *D. pseudoobscura* (unpublished data).

We do not detect Pio protein in tracheal cells prior to mid stage 11 (Figure 4D; Figure S3A). In early stage 11 *pio* mutants, we observed that Dgrip84 localizes correctly to centrioles (Figure S3F). In late stage 11 embryos, Pio protein becomes restricted to the apical part of the cell (Figures 4E, 4F, and 4G, and Jazwinska et al., 2003). In *pio* mutants of late stage 11, Dgrip84 is diffused in the cytoplasm (Figures 4H, 4I, and 5D),

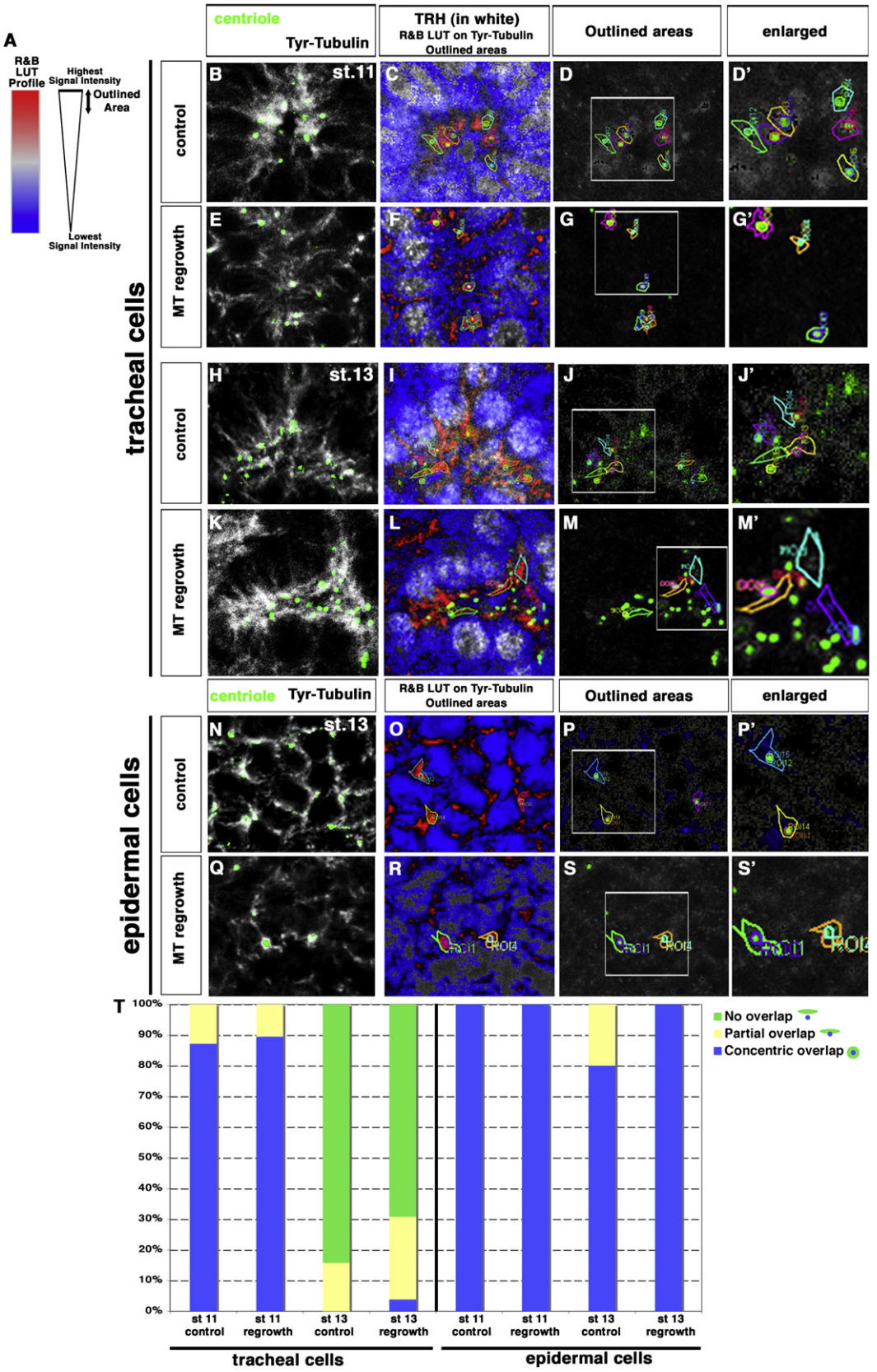
A
R&B LUT Profile
Highest Signal Intensity
Outlined Area
Lowest Signal Intensity
centriole
Tyr-Tubulin
TRH (in white)
R&B LUT on Tyr-Tubulin
Outlined areas
Outlined areas
enlarged
tracheal cells
control
MT regrowth
st.11
st.13
epidermal cells
R&B LUT on Tyr-Tubulin
T
100%
90%
80%
70%
60%
50%
40%
30%
20%
10%
0%
No overlap
Partial overlap
Concentric overlap
st 11 control
st 11 regrowth
st 13 control
st 13 regrowth
tracheal cells
epidermal cells

indicating that γ-TuRC is released from centrosomes but that it is not anchored at the apical site. We can rule out that the lack of γ-TuRC apical anchoring could be explained by the absence of an apical domain in *pio* mutant tracheal cells as the apical marker Crumbs (shown in Jazwinska et al., 2003) and PKC are correctly distributed (Figures S3D and S3E). Thus, Pio is required for γ-TuRC apical anchoring. However, another independent mechanism must regulate γ-TuRC release from the centrosomes.

Spastin Contributes to the γ-TuRC Releasing from Centriole

For that reason, we examined the role of Spas, a member of the microtubule-severing AAA ATPases superfamily (Roll-Mecak and Vale, 2005, 2008), which partially localizes to centrosomes in Cos7 and SK-N-AS cells (Svenson et al., 2005) where it releases MT minus ends (Zhang et al., 2007). Interestingly, Spas is also partially associated with centrosomes in tracheal cells (Figure 5A). We verified that the frequency of overlap between then centriole and Spas is higher that expected by chance (see Experimental Procedures) (Figures S4D–S4F). At late stage 11, when Dgrip84 is mainly apically located in the wild-type, Dgrip84 remains at centrosomes in $spas^{m/z}$ mutant tracheal cells (Figure 5B) in more than 80% of cases (Figure 5D) (see Experimental Procedures for genotype). Concurrently, in the same embryos, γ-tubulin is also detected at centrosomes (Figure 5C). Hence, Spas activity is required for the release of the γ-TuRC from the centrosomes.

We next examined the effect of Spas function on MT organization in tracheal cells. We first looked at the distribution of ace-MTs fibers with respect to the centriole position at stages 11 and 13 (Figures S4G–S4J). While in WT and *pio* mutants ace-MTs fibers are rarely visible in the vicinity of the centriole in the tracheal cells (Figures S4G, S4H, and S4J), ace-MTs fibers of $spas^{m/z}$ embryos are frequently detected close to the centriole (Figures S4I and S4J). We also measured MT levels in $spas^{m/z}$ and wild-type tracheal cells and found a 41% decrease at stage 11 and a 20% decrease at stage 15 in $spas^{m/z}$ compared with the wild-type (Figure S4K). Lower levels of MTs in $spas^{m/z}$ mutants correlate with an increased MT stabilization: at stage 11 there are twice more ace-MT in $spas^{m/z}$ mutants than in wild-type (Figure S4L). We also examined *pio* mutants; at stage 11 the overall MT levels and the ratio of ace-MT are indistinguishable from wild-type (Figure S3G). In contrast, at stage 15, the relative levels of MT in tracheal cells are lower in *pio* mutants compared with the wild-type: the ratio of MT level is 1.65 in the former compared with 2.6 in the latter (Figure S3G) (see Experimental Procedures for details). In addition, and in contrast to the wild-type, stable ace-MTs do not increase in the tracheal cells of *pio* mutants. Thus, Spas and Pio activity are crucial to sustain higher MT levels and to allow MT stabilization (Figures S3G, S4K, and S4L), pointing to a functional role of the relocalization of the MTOC components at the apical membrane.

MTs Are Critical for Tracheal Morphogenesis and for Specific Tracheal Function

To study the functional requirement of MTs in tracheal morphogenesis, we first induced early Spas overexpression (see Experimental Procedures), which leads to depolymerization of most MTs in tracheal cells at stage 11 (Figures 6A′and 6B′). Under these conditions, tracheal placodes invaginate abnormally (Figures 6A–6B″) (80%, n = 15 placodes). As development proceeds, we observe absence of branches, breaks in the tracheal tree (29%, n = 45 metameres) (Figures 6I–6J″ and Figures S5A–S5B″) and defects in lumen formation, as indicated by the low and abnormal deposition of chitin (Figures 6J′ and 6K′). Chitin is synthesized by apically secreted enzymes and its abnormal deposition suggests that the MT dependent membrane transport (Vaughan, 2005) is largely impaired in the absence of MTs. Some MTs are still present upon Spas overexpression (Figures S5A′ and S5A″), which could explain why branch and lumen formation are not totally impaired. We confirmed the tracheal cell-autonomous defect of MT depolymerization with a specific driver that overexpresses Spas only in the tracheal cells, although later and at lower levels, and thus the phenotypes observed were less severe (Figures S5C–S5E″). In a second approach, we used a cold treatment assay, which is reversible and allows the evaluation of both MT disassembly and reassembly. After 6 hr at 4°C, MT fibers are depolymerized in tracheal cells at placode stage (Figures 6C–6D″) and remaining MTs are associated mostly with centrioles (Figures 6C–6D″). Under these conditions, the invaginating placode is disorganized (Figures 6D–6D″). Remarkably, upon MT regrowth, the placode readopts its proper organization (Figures 6F–6F″). In neither of the two assays does MT depletion alter the distribution of adherens junctions (Halbleib and Nelson, 2006) (Figures S5F–S5G″) or apical markers, such as Crumbs and aPKC (Goldstein and Macara, 2007) (Figures 6G–6H″). Similar phenotypes were observed by impairing γ-TuRC with RNAi against *Dgrip84*, *Dgrip163*, and *Dgrip128* or in zygotic *Dgrip84* mutants at late stages (Figures S6H–S6Q″). To more precisely analyze the role of γ-TuRC relocalization, we monitored tracheal morphogenesis in $spas^{m/z}$ embryos. We also observed branch migration and fusion defects (Figure 6L), and lower lumen deposition of chitin, which is also detected in the cytoplasm (Figures 6I′, 6M, and 6M′), thereby suggesting that it was not properly secreted.

Figure 3. MT Nucleation Center Shifts from Centriole Position to Cell Apical Domain during Tracheal Morphogenesis

(A) R&B LUT profile in which maximum and minimum intensity signals appear in red and blue, respectively.

(B–S′) Tyrosinated tubulin detects MTs newly assembled and centrioles are labeled using anti-GFP antibody on asl-YFP embryos.

(B–M′) Tracheal cells of stage 11 (B–G′) and stage 13 (H–M′) are identified by a TRH-positive nuclei pseudocolored in white (C, F, I, and L).

(N–S′) Epidermal cells of stage 13. Controls (B–D′, H–J′, and N–P′) or 2 min MT regrowth after MT depolymerization by cold treatment (E–G′, K–M′, and Q–S′).

(B, E, H, K, N, and Q) Single confocal sections showing Tyr-tubulin staining (in white) and centrioles (in green).

(C, F, I, L, O, and R) R&B LUT applied on Tyr-tubulin signal. Areas corresponding to the maximum intensity signal (in red) are outlined as well as centriole location.

(D, D′, G, G′, J, J′, M, M′, P, P′, S, and S′) Outlined areas only and enlarged views.

(T) Graph showing the percentages of maximum intensity areas overlapping, partially overlapping or not overlapping with centriole position in tracheal and epidermal cells. See also Figure S2.

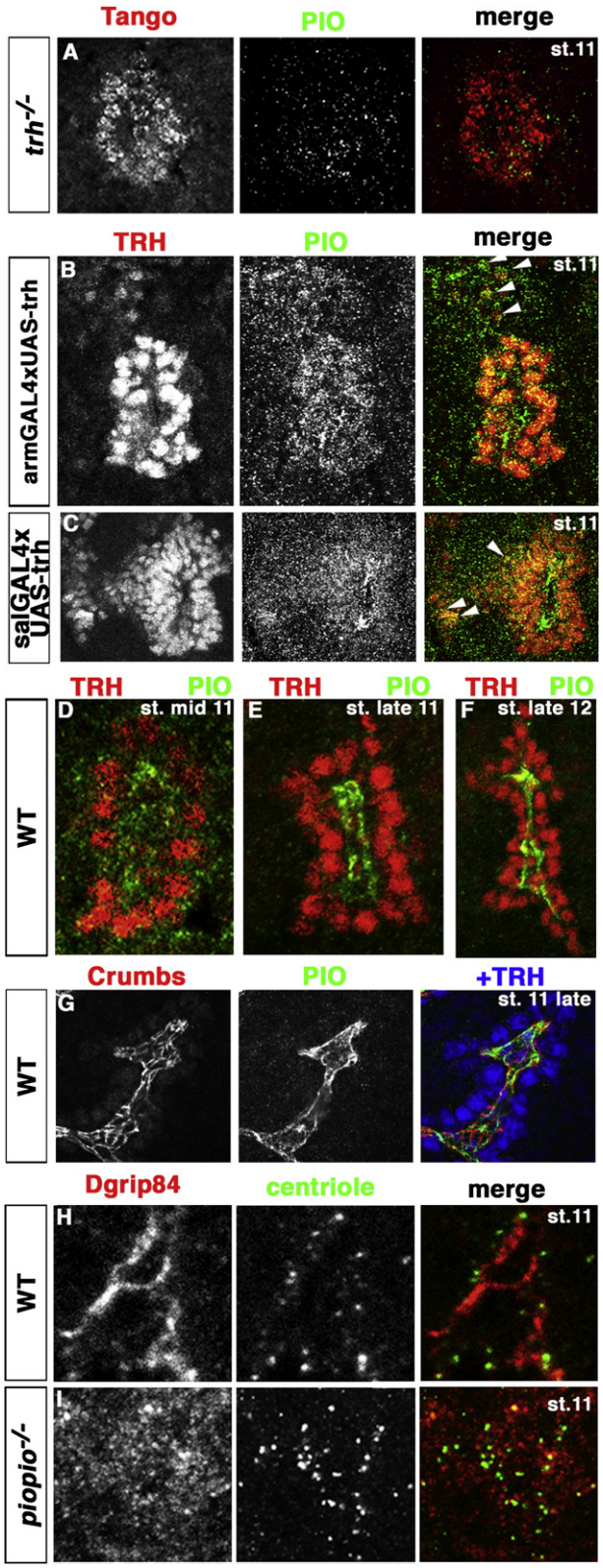

Figure 4. Piopio Is Required for γ-TuRC Apical Anchoring

(A) Pio is not detected in *trh* mutant tracheal cells.

(B and C) By contrast, Trh ectopical-expression, driven by *armGAL4* (B) or *salGAL4* (C), leads to ectopic expression of Pio in epidermal cells (arrowheads).

(D–F) Pio expression in tracheal cells at mid stage 11 (D), late stage 11 (E), and late stage 12 (F).

(G) At late stage 11, Pio localizes with an apical domain containing the Crumbs protein.

(H and I) At stage 11, Dgrip84 localization in tracheal cells of WT (H) and *pio* mutant (I) embryos. Dgrip84 appears diffuse in the cytoplasm of $pio^{-/-}$ tracheal cells. See also Figure S3.

Measurements of MT and ace-MT contents (Figures S4K and S4L) show that lower levels of MTs in $spas^{m/z}$ mutant tracheal cells correlate with an increase in the amount of ace-MTs fibers. Together with the higher number of ace-MTs fibers detected close to centrioles in $spas^{m/z}$ mutants (Figures S4I and S4J), these results illustrate how perturbing MTOC relocalization affects MT organization. As a consequence, modifications in MT organization lead to branch malformations and lumen defects in the trachea, two phenotypes described when MTs are depleted. Altogether this demonstrates the importance of the correct organization of the MT network during morphogenesis.

DISCUSSION

In summary, we identify a two-step mechanism that controls γ-TuRC relocalization and MT network reorganization during in vivo development and show that these changes are essential for morphogenesis (Figure 6N). In a first step, Spas releases γ-TuRC from centrioles, probably by severing MTs close to the centrosome, thus stimulating the depolymerization of the MT stubs attached to γ-TuRC and leading to γ-TuRC detachment from centrosomes (Zhang et al., 2007) (Figure 6N). Because Spas shows a normal distribution in *trh* mutants, we speculate that Spas activity, but not its expression, is regulated by *trh*. Another enzyme, Katanin, has been implicated in the release of MTs from the centrosome in neurons (Ahmad et al., 1999). However, two observations indicate that Katanin appears not to have a role in this process. First, we do not see any effect upon expression of a UAS-RNAi construct for *katanin* in tracheal morphogenesis (data not shown). Second, using a Katanin antibody (Zhang et al., 2007), we did not detect Katanin in the tracheal cells (data not shown), which fits with the absence of the RNAi effect in the trachea. Subsequently, γ-TuRC is transported in a MT-dependent manner toward the apical membrane. Further work will be required to elucidate this transport mechanism, but we speculate that upon detachment from centrosome, the γ-TuRC associated with released MT will be directed toward the apical cortex. Interestingly, γ-TuRC has been recently observed along interphasic MTs (Bouissou et al., 2009). In a second step, *trh* controls the expression of Pio, which was known to act as a MT anchor in *Drosophila* wing cells. We thus establish Pio as an intermediate between a cell-fate-inducing gene and MT network reorganization and show that Pio anchoring of MTs is linked to its ability to act as a γ-TuRC apical anchor.

Regulation of the MT network is likely to be an essential step in morphogenesis, and previous studies have shown that signaling pathways such as Decapentaplegic (Shen and Dahmann, 2005) and Hedgehog (Corrigall et al., 2007) affect MT organization. However, the molecular effectors responsible for the MT

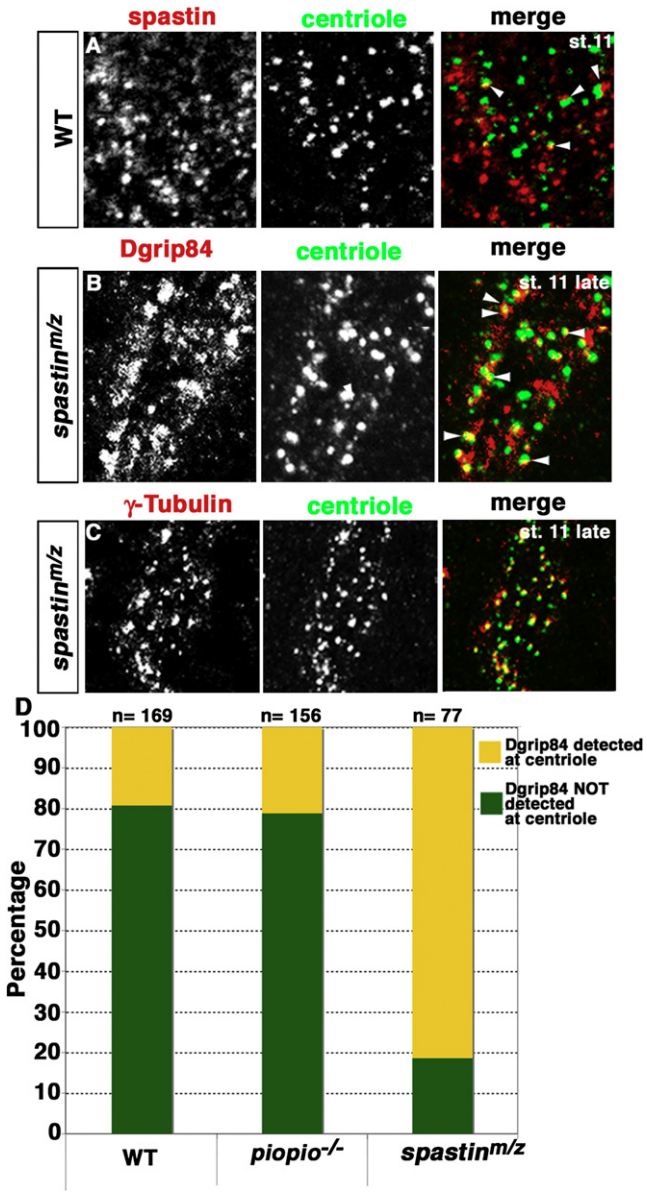

Figure 5. Spastin Is Required for γ-TuRC Release from the Centriole

(A) Spas distribution at stage 11 in tracheal cells. In part, Spas closely associates with centrioles (arrowheads).

(B) In contrast to WT, Dgrip84 largely colocalizes with the centriole position in *spas*$^{m/z}$ tracheal cells (arrowheads) and apical distribution is much affected.

(C) In the tracheal cells of stage 11 of *spas*$^{m/z}$ embryos, γ-tubulin localization is detected at centrioles as opposed to WT embryos.

(D) Graph showing the percentages of centrioles colocalizing and not colocalizing with Dgrip84 in WT, *pio*$^{-/-}$, and *spas*$^{m/z}$ contexts. See also Figure S4.

changes were not identified. Here, we unveil the molecular mechanisms triggered by the *trh* transcription factor to induce the apical relocalization of the γ-TuRC and the MT network reorganization during tracheal morphogenesis.

Although the apical relocalization of MT nucleation activity takes place in tracheal cells, our results show that centrosomes continue to act as MTOCs in neighboring epithelial cells. This is in contrast to what happens in cells of the amnioserosa and leading edge cells during dorsal closure in late *Drosophila* embryogenesis. In both these cell types, the centrosomes do not function as MTOCs (Jankovics and Brunner, 2006; Rogers et al., 2008), although the mechanisms required for switching from centrosomal to noncentrosomal MT nucleation are not understood. Differences between centrosome nucleation activity in early epithelial cells (stage 13) and in the amnioserosa and leading edge cells could be related to their developmental stage and extent of differentiation.

Apical MT anchorage is a common feature of epithelial structures (Meads and Schroer, 1995) (Mogensen, 1999) and, as in tracheal cells, is associated with more stable MTs in many cell types (Keating and Borisy, 1999). However, the way in which this process occurs and its function are not well understood. Thus, in some cases, MT nucleation could still occur at the centrosome and subsequently MTs would be released and apically anchored. Consistent with this possibility, the vertebrate protein Ninein, which participates in the docking of γ-TuRC to the centrosome (Delgehyr et al., 2005), is translocated to the apical cell domain in some epithelial cells where it then anchors the MT minus ends independent of γ-TuRC, which remains associated with centrosomes (Lechler and Fuchs, 2007). Conversely, in neural tube development, the *Xenopus* Shroom protein participates in the establishment of an apical MT array and controls apical redistribution of γ-tubulin (Lee et al., 2007). Similarly, γ-tubulin and some MTOC markers are located apically in vertebrate lens cells (Dahm et al., 2007). Although the mechanisms triggering apical MT redistribution are not well known in theses cases, Shroom and related proteins might play a similar role to Pio. In this regard, it is also worth mentioning that Endoglin, the mammalian protein most similar to Pio, is reported to be essential for angiogenesis in the mouse. This process has been found to share many similarities with tracheal development (Jazwinska et al., 2003). More precisely, both Endoglin and Pio have a conserved short C-terminal domain together with a ZP domain in the extracellular domain. In addition, the Endoglin cytoplasmic domain interacts with MT-associated proteins (Meng et al., 2006) and thus, in mammals, Endoglin could also have a similar role to Pio. Therefore, a two-step process combining the control of MT severing activity in the centrosome with the regulation of a spatially restricted anchoring protein might be a general mechanism to trigger the relocalization of MTOC components and to reorganize the MT network, and consequently to enable specific cell functions and morphogenesis.

EXPERIMENTAL PROCEDURES

Fly Strains

A description of most of the genetic elements can be found at http://flybase.net (FlyBase Consortium, 1999). *Drosophila* stocks and crosses were kept under standard conditions at 25°C. The asl-YFP transgenic line was used to detect centriole position (Varmark et al., 2007). The following loss-of-function mutations were used: *trh*^{1}, *pio*^{2R16} (Jazwinska et al., 2003), *Dgrip84*^{R20} (Colombie et al., 2006), *spas*$^{5.75}$ (Sherwood et al., 2004). FM7-*ftz-lacZ,* CyO-*wg-lacZ*, TM3-*ftz-lacZ*, or TM6-*Ubx-lacZ* blue balancers were used to identify homozygous embryos. In *Drosophila*, *spas* has a large maternal contribution and zygotic mutants do not have any tracheal phenotype. Thus, to test Spas function, we examined embryos maternally and zygotically mutant for *spas*, referred to as *spas*$^{m/z}$. Germline

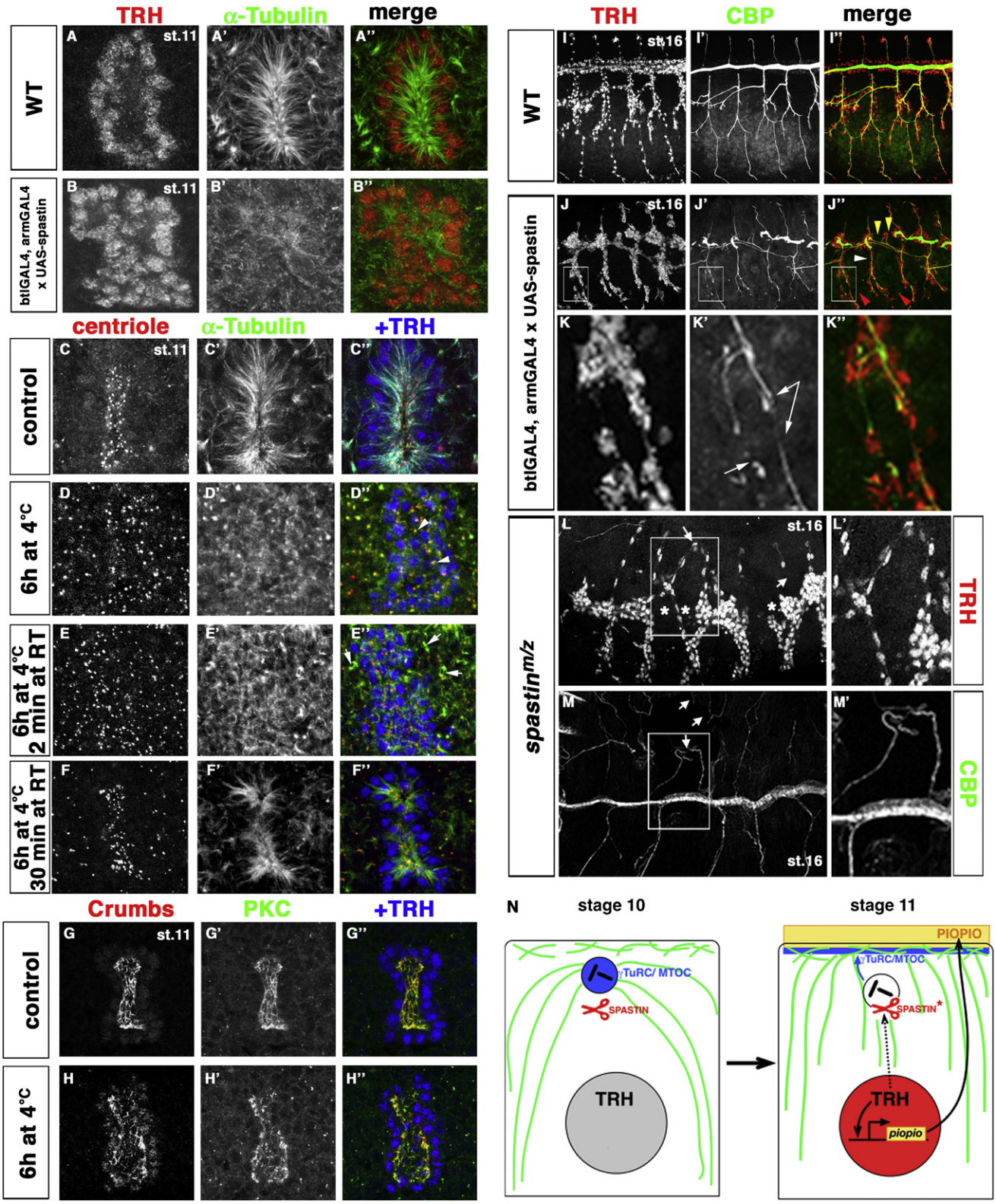

Figure 6. MTs Are Critical for Specific Tracheal Function and Tracheal Morphogenesis

(A–B″) Spas overexpression, driven by both *btlGAL4* and *armGAL4*, leads to almost complete MT depolymerization (A′, B′). At stage 11, after MT depletion, the tracheal placode lacks its characteristic "finger-like" structure (A, B).

clones were generated by the FLP/FRT technique (Chou et al., 1993) using the following lines: *w[*]; P{neoFRT}82B P{ovoD1-18}3R/st[1] betaTub85D[D] ss[1] e[s]*/TM3,*Sb[1]*, P{*hsFLP*}*1*, *y[1] w[1118]; Dr[1]/TM3,Sb[1]*, P{*neoFRT*}*82B Spastin*/TM3-*ftz-lacZ*. We used the GAL4 system (Brand and Perrimon, 1993) for misexpression experiments. The *armGAL4* (Vincent et al., 1994), *btlGAL4* (Shiga et al., 1996) and *salGAL4* (Boube et al., 2000) lines were used at 29°C in combination with UAS-*spastin*-EGFP (Trotta et al., 2004), UAS-*trh* (Wilk et al., 1996), UAS-*Dgrip84*-RNAi, UAS-*Dgrip128*-RNAi, UAS-*Dgrip163*-RNAi (VDRC consortium, Dietzl et al., 2007).

Immunohistochemistry

Embryos were staged as described elsewhere (Campos-Ortega and Hartenstein, 1985) and fixed and stained following standard protocols. To visualize MTs, embryos were fixed for 10 min as described previously (Lee et al., 2003). Primary antibodies were as described elsewhere (Brodu and Casanova, 2006) with the following additions: anti-Crumbs (1:10, Cq4 DSHB), anti-α−Catenin (1:20, DCAT-1 DSHB), anti-Pio (1:20, (Jazwinska et al., 2003)), anti-α−tubulin-FITC and anti-acetyl-tubulin (1:200, Sigma) anti-tyrosine-tubulin (1:200, Tyr1/2 Abcam), and γ-tubulin specifically directed against *D. melanogaster* γ-tubulin 23C (1:500, R62 [Raynaud-Messina et al., 2001]), anti-Dgrip84 (1:1000, R67 [Colombie et al., 2006]), anti-Dgrip75 (1:200, Schnorrer et al., 2002), anti-Dgrip163 (1:100, Gunawardane et al., 2000), anti-Spas (1:200, Zhang et al., 2007), anti-CP309 (1:1000, our own stock). Alexa Fluor 405, Cy2, Cy3, and Cy5 secondary antibodies (Invitrogen and Jackson ImmunoResearch, respectively) were used at a dilution of 1:200. DAPI was used for DNA detection. Tracheal cells were identified either using antibodies against transcription factors Tango or Trh. Tango has been shown to dimerize in vivo with Trh. As a heterodimer, Trh functions to specify trachea cell fate. Anti-spectrin labels cell membrane and anti-α−tubulin labels MT network. Centrioles were detected using anti-GFP antibody on asl-YFP embryos or using an antibody against CP309, a constitutive pancentriolar protein. All fluorescent images were collected using confocal microscopy (Leica TCS-SP5-AOBS system, Leica DMI6000B microscope and Leica confocal software [LAS-AF 1.7.0]) and processed using ImageJ and Photoshop (Adobe Photosystems). These images are projections of two consecutive confocal sections, except for Figures 2A–2A‴, 3B, 3E, 3H, 3K, 3N, 3Q, and 5A and Figures S4D–S4F, which show single confocal sections, and Figures S6A–S6E, S6I, S6K, S6M, S6O, and S6P, which show projections of several confocal sections.

Image Processing and MT Quantification

Embryos from overnight collections were fixed for MTs and stained with α−tubulin, acetylated tubulin, and tyrosinated tubulin antibodies. Images were acquired, for a given antibody, using the same confocal settings through different stages. Quantification of α-tubulin, acetylated, and tyrosinated tubulin signal intensity was performed on a single confocal section using the "integrate density" function of ImageJ. ROI corresponding to one cell area was defined and signal intensity, reflecting the amount of α-tubulin, acetylated tubulin, and tyrosinated tubulin, was determined. This operation was repeated for 35–76 cells of the same confocal section and through two or three sections. To compare values between sections, we integrated the decrease in signal intensity along the Z-axis. To do so, we measured the decrease in signal intensity along the Z-axis for ubiquitous and uniformly expressed markers such as neurotactin, spectrin, and DAPI. We then extrapolated value intensity depending on the Z-axis [value intensity = 0.7639 * exp(0.1128 * (Z step)]. It is worth noting that signal intensity depends on confocal settings defined for a given antibody, thereby explaining why ratios can be above 1. Error bars indicate standard deviation. For *pio* mutant embryos, we quantified overall MT levels and ace-MT levels in $pio^{-/-}$ tracheal cells with respect to epidermal cells. *pio* is not expressed in epidermal cells and changes in these ratios reveal a specific change in tracheal cells. For $spas^{m/z}$ mutant embryos, we compared MT levels and ace-MT levels between wild-type and $spas^{m/z}$ tracheal cells.

To define the MT nucleation center, we applied, on raw images using LAS-AF software, the R&B LUT in which the signal of maximum and minimum intensity appears in red and blue, respectively. We then delineated areas corresponding to this maximum intensity signal for tyr-Tub staining and measured surface area. We also measured centriole surface, which remained constant throughout development.

MT Disassembly and Regrowth

For maximum MT depolymerization, embryos were collected overnight at 25°C, dechorionated with 50% bleach, and incubated on ice for 6 hr. To follow MT regrowth, embryos were subsequently incubated at 25°C for 2 min or 30 min. Control embryos were processed in a similar way but kept for 6 hr at 25°C. Embryos were then fixed as described previously (Lee et al., 2003) and stained for MTs.

Measure of Overlap Frequency between Centrioles and Spas Dots

We quantified the frequency of overlap between centrioles and Spas dots and measured that 32% of centrioles dots overlap with Spas dots. To assess that this overlap is higher than expected by chance, we calculated the frequency of overlap when centriole channel had been rotated clockwise. Overlap frequency was dropped to 1.7% as compared with controls, clearly indicating that Spas and centriole colocalization is not random.

SUPPLEMENTAL INFORMATION

Supplemental Information includes six figures and can be found with this article online at doi:10.1016/j.devcel.2010.03.015.

ACKNOWLEDGMENTS

We thank the Imaging Facilities at "Institut Jacques Monod," in particular T. Piolot and V. Contremoulins, for assistance with image quantification; M. Affolter, D. Brunner, C. Gonzalez, B. Raynaud-Messina, D. Sharp, F. Schnorrer, N. Sherwood, and Y. Zheng for reagents; and R. Basto, M. Bornens, Kyra Campbell, L. Gervais, C. Gonzalez, J. Lüders, and D. Shaye for critical discussions and reading of the manuscript. This work was supported by grants from the CNRS and ANR « Blanche » (grant Cymempol, Blan06-3-139786). J.C. is supported by the Generalitat de Catalunya, the Spanish Ministerio de Ciencia e Innovación, and its Consolider-Ingenio 2010 program.

(C–F″) After a 6 hr incubation at 4°C (D″), MTs are largely depolymerised (compare C′ with D′), leading to disorganization of the tracheal placode. The only remaining MTs are associated with centrioles (arrowheads in D″). After 2 min at room temperature (RT) (E″), MTs start regrowing, which is illustrated by the resuming of cell division in epithelial cells (white arrow in [E″]). After 30 min at RT (F″), MTs have fully regrown and the tracheal placode regains its original shape. Here centrioles are detected with asl-YFP transgene.

(G and H) MT depletion does not affect cell polarity as Crumbs (G and H) and aPKC (G′ and H′) localizations remain apical in WT (G″) and after 6 hr at 4°C (H″).

(I–K″) Spas overexpression produces branch breaks, resulting from either absence of fusion (red arrowhead in [J″]), or from a failure of cell migration (yellow arrowhead in [J]).Visceral branches are often missing (white arrowhead in [J″]). Lumen product secretion, revealed by CBP, is continuous in all branches in WT (I′). In contrast, Spas overexpression leads to a reduction in CBP secretion levels. Gaps are observed (white arrows in [K″]), indicating that lumen is not uniformly secreted.

(L and M) Tracheal phenotypes in $spas^{m/z}$ embryos at stage 16 showing lack of branch migration (asterisks in [L]) and branch misrouting (arrows in [L] and [M]). CBP secretion is not uniform and lower than in WT.

(N) A model for the two-step process controlling the translocation of MT nucleation activity in tracheal cells. At stage 10, epidermal cells acquire tracheal cell fate upon *trh* expression. MTs are nucleated from γ-TuRC containing centrosome. At stage 11, TRH (dashed line) modulates Spas activity (now Spastin*) either by a change in Spastin itself or another component required for its activity. In addition, TRH activates *pio* expression. Pio is an apically localized transmembrane protein. First, Spastin* triggers γ-TuRC release from the centriole and the γ-TuRC is then transported via MT motors toward the apical membrane (blue arrow). Second, Pio anchors the γ-TuRC apically. MTs are then nucleated from the apical domain. See also Figure S5.

Received: September 5, 2009
Revised: January 22, 2010
Accepted: March 12, 2010
Published: May 17, 2010

REFERENCES

Affolter, M., Bellusci, S., Itoh, N., Shilo, B., Thiery, J.P., and Werb, Z. (2003). Tube or not tube: remodeling epithelial tissues by branching morphogenesis. Dev. Cell *4*, 11–18.

Ahmad, F.J., Yu, W., McNally, F.J., and Baas, P.W. (1999). An essential role for katanin in severing microtubules in the neuron. J. Cell Biol. *145*, 305–315.

Bartolini, F., and Gundersen, G.G. (2006). Generation of noncentrosomal microtubule arrays. J. Cell Sci. *119*, 4155–4163.

Bokel, C., Prokop, A., and Brown, N.H. (2005). Papillote and Piopio: Drosophila ZP-domain proteins required for cell adhesion to the apical extracellular matrix and microtubule organization. J. Cell Sci. *118*, 633–642.

Boube, M., Llimargas, M., and Casanova, J. (2000). Cross-regulatory interactions among tracheal genes support a co-operative model for the induction of tracheal fates in the Drosophila embryo. Mech. Dev. *91*, 271–278.

Bouissou, A., Verollet, C., Sousa, A., Sampaio, P., Wright, M., Sunkel, C.E., Merdes, A., and Raynaud-Messina, B. (2009). {gamma}-Tubulin ring complexes regulate microtubule plus end dynamics. J. Cell Biol. *187*, 327–334.

Brand, A.H., and Perrimon, N. (1993). Targeted gene expression as a means of altering cell fates and generating dominant phenotypes. Development *118*, 401–415.

Brodu, V., and Casanova, J. (2006). The RhoGAP crossveinless-c links trachealess and EGFR signaling to cell shape remodeling in Drosophila tracheal invagination. Genes Dev. *20*, 1817–1828.

Campos-Ortega, A.J., and Hartenstein, V. (1985). The Embryonic Development of Drosophila melanogaster (New York: Springer-Verlag).

Chou, T.B., Noll, E., and Perrimon, N. (1993). Autosomal P[ovoD1] dominant female-sterile insertions in Drosophila and their use in generating germ-line chimeras. Development *119*, 1359–1369.

Colombie, N., Verollet, C., Sampaio, P., Moisand, A., Sunkel, C., Bourbon, H.M., Wright, M., and Raynaud-Messina, B. (2006). The Drosophila gamma-tubulin small complex subunit Dgrip84 is required for structural and functional integrity of the spindle apparatus. Mol. Biol. Cell *17*, 272–282.

Corrigall, D., Walther, R.F., Rodriguez, L., Fichelson, P., and Pichaud, F. (2007). Hedgehog signaling is a principal inducer of Myosin-II-driven cell ingression in Drosophila epithelia. Dev. Cell *13*, 730–742.

Dahm, R., Procter, J.E., Ireland, M.E., Lo, W.K., Mogensen, M.M., Quinlan, R.A., and Prescott, A.R. (2007). Reorganization of centrosomal marker proteins coincides with epithelial cell differentiation in the vertebrate lens. Exp. Eye Res. *85*, 696–713.

Delgehyr, N., Sillibourne, J., and Bornens, M. (2005). Microtubule nucleation and anchoring at the centrosome are independent processes linked by ninein function. J. Cell Sci. *118*, 1565–1575.

Dietzl, G., Chen, D., Schnorrer, F., Su, K.C., Barinova, Y., Fellner, M., Gasser, B., Kinsey, K., Oppel, S., Scheiblauer, S., et al. (2007). A genome-wide transgenic RNAi library for conditional gene inactivation in Drosophila. Nature *448*, 151–156.

Goldstein, B., and Macara, I.G. (2007). The PAR proteins: fundamental players in animal cell polarization. Dev. Cell *13*, 609–622.

Gunawardane, R.N., Martin, O.C., Cao, K., Zhang, L., Dej, K., Iwamatsu, A., and Zheng, Y. (2000). Characterization and reconstitution of Drosophila gamma-tubulin ring complex subunits. J. Cell Biol. *151*, 1513–1524.

Halbleib, J.M., and Nelson, W.J. (2006). Cadherins in development: cell adhesion, sorting, and tissue morphogenesis. Genes Dev. *20*, 3199–3214.

Hammond, J.W., Cai, D., and Verhey, K.J. (2008). Tubulin modifications and their cellular functions. Curr. Opin. Cell Biol. *20*, 71–76.

Isaac, D.D., and Andrew, D.J. (1996). Tubulogenesis in Drosophila: a requirement for the trachealess gene product. Genes Dev. *10*, 103–117.

Jankovics, F., and Brunner, D. (2006). Transiently reorganized microtubules are essential for zippering during dorsal closure in Drosophila melanogaster. Dev. Cell *11*, 375–385.

Jazwinska, A., Ribeiro, C., and Affolter, M. (2003). Epithelial tube morphogenesis during Drosophila tracheal development requires Piopio, a luminal ZP protein. Nat. Cell Biol. *5*, 895–901.

Keating, T.J., and Borisy, G.G. (1999). Centrosomal and non-centrosomal microtubules. Biol. Cell *91*, 321–329.

Lechler, T., and Fuchs, E. (2007). Desmoplakin: an unexpected regulator of microtubule organization in the epidermis. J. Cell Biol. *176*, 147–154.

Lee, M., Lee, S., Zadeh, A.D., and Kolodziej, P.A. (2003). Distinct sites in E-cadherin regulate different steps in Drosophila tracheal tube fusion. Development *130*, 5989–5999.

Lee, C., Scherr, H.M., and Wallingford, J.B. (2007). Shroom family proteins regulate gamma-tubulin distribution and microtubule architecture during epithelial cell shape change. Development *134*, 1431–1441.

Meads, T., and Schroer, T.A. (1995). Polarity and nucleation of microtubules in polarized epithelial cells. Cell Motil. Cytoskeleton *32*, 273–288.

Meng, Q., Lux, A., Holloschi, A., Li, J., Hughes, J.M., Foerg, T., McCarthy, J.E., Heagerty, A.M., Kioschis, P., Hafner, M., and Garland, J.M. (2006). Identification of Tctex2beta, a novel dynein light chain family member that interacts with different transforming growth factor-beta receptors. J. Biol. Chem. *281*, 37069–37080.

Mogensen, M.M. (1999). Microtubule release and capture in epithelial cells. Biol. Cell *91*, 331–341.

Oegema, K., Wiese, C., Martin, O.C., Milligan, R.A., Iwamatsu, A., Mitchison, T.J., and Zheng, Y. (1999). Characterization of two related Drosophila gamma-tubulin complexes that differ in their ability to nucleate microtubules. J. Cell Biol. *144*, 721–733.

Pickett-Heaps, J. (1971). The autonomy of the centriole: fact or fallacy? Cytobios *3*, 205–214.

Raynaud-Messina, B., and Merdes, A. (2007). Gamma-tubulin complexes and microtubule organization. Curr. Opin. Cell Biol. *19*, 24–30.

Raynaud-Messina, B., Debec, A., Tollon, Y., Gares, M., and Wright, M. (2001). Differential properties of the two Drosophila gamma-tubulin isotypes. Eur. J. Cell Biol. *80*, 643–649.

Rogers, G.C., Rusan, N.M., Peifer, M., and Rogers, S.L. (2008). A multicomponent assembly pathway contributes to the formation of acentrosomal microtubule arrays in interphase Drosophila cells. Mol. Biol. Cell *19*, 3163–3178.

Roll-Mecak, A., and Vale, R.D. (2005). The Drosophila homologue of the hereditary spastic paraplegia protein, spastin, severs and disassembles microtubules. Curr. Biol. *15*, 650–655.

Roll-Mecak, A., and Vale, R.D. (2008). Structural basis of microtubule severing by the hereditary spastic paraplegia protein spastin. Nature *451*, 363–367.

Schnorrer, F., Luschnig, S., Koch, I., and Nusslein-Volhard, C. (2002). Gamma-tubulin37C and gamma-tubulin ring complex protein 75 are essential for bicoid RNA localization during drosophila oogenesis. Dev. Cell *3*, 685–696.

Shen, J., and Dahmann, C. (2005). Extrusion of cells with inappropriate Dpp signaling from Drosophila wing disc epithelia. Science *307*, 1789–1790.

Sherwood, N.T., Sun, Q., Xue, M., Zhang, B., and Zinn, K. (2004). Drosophila spastin regulates synaptic microtubule networks and is required for normal motor function. PLoS Biol. *2*, e429.

Shiga, Y., Tanaka-Matakatsu, M., and Hayashi, S. (1996). A nuclear GFP/β-galactosidase fusion protein as a marker for morphogenesis in living *Drosophila*. Dev. Growth Differ. *38*, 99–106.

Svenson, I.K., Kloos, M.T., Jacon, A., Gallione, C., Horton, A.C., Pericak-Vance, M.A., Ehlers, M.D., and Marchuk, D.A. (2005). Subcellular localization of spastin: implications for the pathogenesis of hereditary spastic paraplegia. Neurogenetics *6*, 135–141.

Trotta, N., Orso, G., Rossetto, M.G., Daga, A., and Broadie, K. (2004). The hereditary spastic paraplegia gene, spastin, regulates microtubule stability to modulate synaptic structure and function. Curr. Biol. *14*, 1135–1147.

Uv, A., Cantera, R., and Samakovlis, C. (2003). Drosophila tracheal morphogenesis: intricate cellular solutions to basic plumbing problems. Trends Cell Biol. *13*, 301–309.

Varmark, H., Llamazares, S., Rebollo, E., Lange, B., Reina, J., Schwarz, H., and Gonzalez, C. (2007). Asterless is a centriolar protein required for centrosome function and embryo development in Drosophila. Curr. Biol. *17*, 1735–1745.

Vaughan, K.T. (2005). Microtubule plus ends, motors, and traffic of Golgi membranes. Biochim. Biophys. Acta *1744*, 316–324.

Verollet, C., Colombie, N., Daubon, T., Bourbon, H.M., Wright, M., and Raynaud-Messina, B. (2006). Drosophila melanogaster gamma-TuRC is dispensable for targeting gamma-tubulin to the centrosome and microtubule nucleation. J. Cell Biol. *172*, 517–528.

Vincent, J.P., Girdham, C.H., and O'Farrell, P.H. (1994). A cell-autonomous, ubiquitous marker for the analysis of Drosophila genetic mosaics. Dev. Biol. *164*, 328–331.

Wiese, C., and Zheng, Y. (2006). Microtubule nucleation: gamma-tubulin and beyond. J. Cell Sci. *119*, 4143–4153.

Wilk, R., Weizman, I., and Shilo, B.Z. (1996). trachealess encodes a bHLH-PAS protein that is an inducer of tracheal cell fates in Drosophila. Genes Dev. *10*, 93–102.

Zhang, D., Rogers, G.C., Buster, D.W., and Sharp, D.J. (2007). Three microtubule severing enzymes contribute to the "Pacman-flux" machinery that moves chromosomes. J. Cell Biol. *177*, 231–242.